JOURNAL OF AIRCRAFT
Vol. 46, No. 4, July–August 2009

System Identification of a Miniature Helicopter

J. Grauer,* J. Conroy,* J. Hubbard Jr.,† J. Humbert,‡ and D. Pines§
University of Maryland, College Park, Maryland 20742

DOI: 10.2514/1.40561

Miniature helicopters provide a unique design choice for performing missions autonomously, vital to which is knowledge of a dynamic model to enable the development of control and state estimation algorithms. Toward these goals, a linear model for a miniature electric helicopter in hovering flight was identified from data obtained from a visual positioning system. Model structure determination was performed using first principles, previous work, and stepwise regression. Model parameters were computed using a two-step equation-error/output-error process in both the time and frequency domains, resulting in two complete sets of parameter estimates. Modal characteristics and predictive capability of the identified models were compared with those of a model previously identified for this aircraft using the frequency-response method.

Nomenclature

A, B	=	main rotor stability derivatives
a, b	=	main rotor flapping angles
g	=	gravitational acceleration
$J(\boldsymbol{\theta})$	=	cost function
j	=	imaginary number
L, M, N	=	moment stability derivatives
N_p	=	number of data points
N_o	=	number of outputs
p, q, r	=	rotational velocity projections
$\mathbf{R}$	=	residual covariance matrix
$\mathbf{S}$	=	residual spectral density matrix
$s(\hat{\boldsymbol{\theta}})$	=	sample standard error
T, X, Y, Z	=	force stability derivatives
t	=	time
$\mathbf{u}$	=	input vector
u, v, w	=	translational velocity projections
x, y, z	=	position projections
$\mathbf{y}$	=	model output vector
$\mathbf{z}$	=	measurement vector
δ	=	pilot control input
ζ, ω	=	modal damping ratio and frequency
$\boldsymbol{\theta}$	=	model parameter vector
$\boldsymbol{v}$	=	residual vector
σ	=	standard deviation
τ	=	main rotor time constant
ϕ, θ, ψ	=	Euler angles
Ω	=	main rotor rotational speed

Subscripts

dir	=	directional
lat	=	lateral cyclic
lon	=	longitudinal cyclic
thr	=	throttle

Superscripts

T	=	transpose
†	=	complex conjugate transpose
-1	=	inverse
~	=	Fourier transform
^	=	estimated value
·	=	time derivative

Presented as Paper 6898 at the AIAA Atmospheric Flight Mechanics Conference and Exhibit, Honolulu, HI, 18–21 August 2008; received 23 August 2008; accepted for publication 14 February 2009.

*Graduate Student, Department of Aerospace Engineering. Member AIAA.

†Langley Distinguished Professor, Department of Aerospace Engineering. Associate Fellow AIAA.

‡Assistant Professor, Department of Aerospace Engineering. Senior Member AIAA.

§Professor, Department of Aerospace Engineering. Associate Fellow AIAA.

I. Introduction

IN RECENT years, there has been a large effort to develop and mature miniature air vehicle platforms for performing autonomous surveillance and reconnaissance missions. Miniature helicopters provide a unique choice because they are highly maneuverable and are capable of hovering flight, making them ideal for flying in confined environments while streaming visual and sensor information to a ground station. Autonomous flight is not only desired, but also necessitated by these missions due to the fast and unstable dynamics of the aircraft, which are exacerbated by any transmission delays of sensor data and control inputs. Canonical linear, time-invariant, state-space models of the dynamics about trimmed flight conditions facilitate the use of modern control and state estimation algorithms which enable autonomous operation.

In comparison with conventional fixed-wing aircraft, obtaining a state-space model for rotary-wing aircraft is significantly more difficult [1,2]. Helicopter rotors add dynamics that couple with the rigid body fuselage motions and the surrounding flowfield, introducing complex and unsteady aerodynamics which manifest in part as rotor/wake and rotor/fuselage interactions [3]. The rotor dynamics also exhibit a large degree of interaxis couplings and higher harmonic

Fig. 1 Helicopter test aircraft.

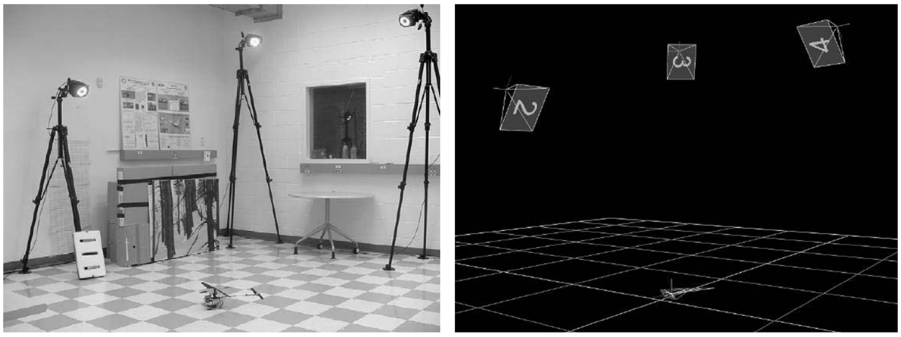

a) Visual image b) Processed image

Fig. 2 Visual positioning system configuration.

responses that compete with requirements for an accurate, low-order model for hardware implementation. Modeling from first principles offers insight into the dynamics, but often requires numerous and drastic simplifications to obtain tractable models. Additionally, the hover dynamics of a helicopter are unstable, often requiring feedback to decrease the pilot workload, which masks the natural dynamics of the system and introduces collinearity into the flight data. The identification of miniature helicopters is further complicated by a number of obstacles. Onboard sensors are typically based on microelectromechanical systems (MEMS) and are of poorer quality than those used in larger aircraft, characterized by strong temperature dependencies, noisy readings, and calibration biases that exhibit random walk. Smaller vehicle sizes reduce the inertia of the system, which increases the sensitivity to wind gusts and sensor noise within the feedback loops. Miniature helicopters are often flown indoors for this reason, although constraints on the flight space hinder the identification of the low-frequency dynamics, which requires longer durations of excitation for observation.

Despite these obstacles, the system identification of linear models for rotorcraft has become a standardized procedure [4–6], typically performed using the frequency-response method, implemented with the software package CIFER® (Comprehensive Identification from Frequency Responses) [7–9]. Input/output data are used to compute empirical Bode diagrams, which are compared with first principles and a coherence metric to estimate transfer functions and state-space models. This method is well suited to helicopter identification because it removes noise and illuminates modal resonances in a computationally efficient manner that is not affected by the stability of the system. There are, however, several drawbacks to using this approach. The basis of frequency domain techniques limits the identification to linear models, resulting in control and state estimation algorithms designed for small perturbations away from trimmed flight conditions. Relatively large amounts of flight data, which may be too expensive or not possible to obtain, are required to obtain accurate parameter estimates [10]. Additionally, windowing and averaging techniques are required when performing Fourier transforms and estimating spectral densities, which introduce engineering judgements into the analysis.

In contrast, system identification of fixed-wing aircraft is most commonly performed using various formulations of the maximum likelihood estimator. Specifically the output-error (OE) method is most prevalent, and has been shown to have good convergence rates given a priori information from an equation-error (EE) analysis [10,11]. This work presents the identification of a linear model describing the hover dynamics of a miniature electric helicopter for the purpose of controller and observer design. Model structure determination is performed using first principles, previous work, and stepwise regression. Model parameters are estimated using the two-step EE/OE approach formulated in both the time and frequency domains, which results in two complete sets of parameter estimates. Modal characteristics and predictive capabilities of the identified models are discussed and compared with a previously identified model for this aircraft (Conroy et al. [12]), which used the frequency-response method and the CIFER® software package. The signal processing and system identification software used in this work are found in a MATLAB® package[¶] called SIDPAC (System Identification Programs for Aircraft) [13,14].

II. Experimental Setup

The test aircraft used in this study was the commercially available HoneyBee helicopter by E-Sky, shown in Fig. 1. The helicopter is a 390 g electric hobby aircraft, with a main rotor diameter of 0.5050 m and a tail rotor diameter of 0.1450 m. Actuator inputs include the throttle input $\delta_{\text{thr}} \in [0, 1]$, which commands the speed of a dc motor attached to the main rotor, cyclic inputs $\delta_{\text{lon}}, \delta_{\text{lat}} \in [-1, +1]$, which command servo motors and position longitudinal and lateral pitch linkages in a Hiller-style stabilizer mechanism, and the directional input $\delta_{\text{dir}} \in [0, 1]$, which commands the speed of a dc motor connected to the tail rotor.

The helicopter was fitted with a custom flight control system (FCS) [12] which was used to stream information from onboard MEMS sensors including magnetometers, gyroscopes, and accelerometers. Additionally, the onboard hardware was used to mix the directional control input with the yaw rate and the throttle input to better pilot the maneuvers at the expense of correlating the data. A commercially available visual positioning system (VPS) was also employed during flight testing.[**] Six cameras were placed around the room and, after a calibration procedure using a known object, the supplied software was used to track the spatial position of numerous retroreflective markers placed on the vehicle. A rigid body mapping of the markers was created in the software so that least-squares estimates of the center of mass position, fuselage orientation, and rotor azimuth angle could be estimated and recorded at 350 Hz. An image of the laboratory and the corresponding image used in the processing software is shown in Fig. 2, displaying the vehicle and three cameras.

Although data were recorded from both the onboard FCS and the VPS, several reasons led to discarding the FCS data for system identification and using instead measurements of the velocity and acceleration derived from the VPS data. The position information from the VPS is based on optical measurements rather than MEMS technology and used a least-squares fit to several markers, averaging out structural vibrations registered by discrete onboard sensors. Deriving velocity and acceleration information from the VPS data circumvented a kinematic consistency analysis and resulted in a data set that produced better modeling results. Additionally, derived acceleration measurements did not require corrections for gravitational and rotational accelerations. A comparison of pitch rate and heave acceleration measurements from the FCS and VPS are shown in Fig. 3. Consistent with the data shown in this work, measurements were low-pass filtered to 5 Hz using a fixed-weight smoothing algorithm, and numerical differentiation was performed using a smoothed local differentiation method [15,16].

[¶]Data available at www.themathworks.com.

[**]Vicon Motion Systems data available at www.vicon.com.

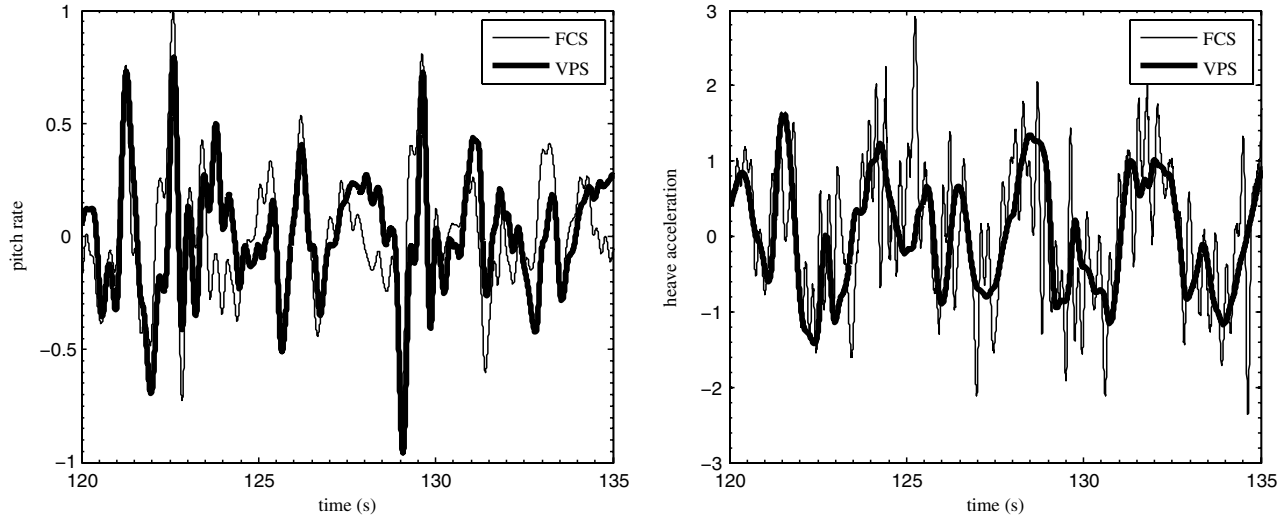

a) Pitch rate **b) Heave acceleration**

Fig. 3 Comparison of FCS and VPS measurements.

The system identification analysis used a control vector consisting of the four pilot joystick inputs, measured after the onboard mixing, and a measurement vector consisting of the roll angle, pitch angle, translational velocities, rotational velocities, and rotor speed. These are written symbolically as

$$\mathbf{u} = [\,\delta_{\text{thr}} \quad \delta_{\text{lon}} \quad \delta_{\text{lat}} \quad \delta_{\text{dir}}\,]^T \tag{1}$$

$$\mathbf{z} = [\,\phi \quad \theta \quad u \quad v \quad w \quad p \quad q \quad r \quad \Omega\,]^T \tag{2}$$

and indicate deviations away from the trimmed values. Orientation is expressed in an inertial frame, whereas velocities are expressed in the aircraft body frame. Sign conventions of the control inputs are assigned such that positive perturbations to the throttle setting, longitudinal cyclic, lateral cyclic, and directional setting primarily induce a negative heave velocity, a negative pitch rate, a negative roll rate, and a negative yaw rate, respectively. Measurement statistics were found from data taken while the helicopter was motionless on the ground and are provided in Table 1, where the units specified are used consistently throughout this work.

$$\begin{bmatrix} \dot{\phi} \\ \dot{\theta} \\ \dot{u} \\ \dot{v} \\ \dot{w} \\ \dot{p} \\ \dot{q} \\ \dot{r} \\ \dot{\Omega} \\ \dot{a} \\ \dot{b} \end{bmatrix} = \begin{bmatrix} 0 & 0 & 0 & 0 & 0 & 1 & 0 & 0 & 0 & 0 & 0 \\ 0 & 0 & 0 & 0 & 0 & 0 & 1 & 0 & 0 & 0 & 0 \\ 0 & -g & X_u & 0 & 0 & 0 & 0 & 0 & 0 & 0 & 0 \\ g & 0 & 0 & Y_v & 0 & 0 & 0 & 0 & 0 & 0 & 0 \\ 0 & 0 & 0 & 0 & Z_w & 0 & 0 & 0 & Z_\Omega & 0 & 0 \\ 0 & 0 & 0 & L_v & 0 & 0 & 0 & 0 & 0 & 0 & L_b \\ 0 & 0 & M_u & 0 & 0 & 0 & 0 & 0 & 0 & M_a & 0 \\ 0 & 0 & 0 & 0 & 0 & 0 & 0 & N_r & 0 & 0 & 0 \\ 0 & 0 & 0 & 0 & 0 & 0 & 0 & 0 & T_\Omega & 0 & 0 \\ 0 & 0 & 0 & 0 & 0 & 0 & -1 & 0 & 0 & -\frac{1}{\tau} & \frac{A_b}{\tau} \\ 0 & 0 & 0 & 0 & 0 & -1 & 0 & 0 & 0 & \frac{B_a}{\tau} & -\frac{1}{\tau} \end{bmatrix} \begin{bmatrix} \phi \\ \theta \\ u \\ v \\ w \\ p \\ q \\ r \\ \Omega \\ a \\ b \end{bmatrix} + \begin{bmatrix} 0 & 0 & 0 & 0 \\ 0 & 0 & 0 & 0 \\ 0 & 0 & 0 & 0 \\ 0 & 0 & 0 & 0 \\ 0 & 0 & 0 & 0 \\ 0 & 0 & 0 & 0 \\ 0 & 0 & 0 & 0 \\ N_{\text{thr}} & 0 & 0 & N_{\text{dir}} \\ T_{\text{thr}} & 0 & 0 & 0 \\ 0 & \frac{A_{\text{lon}}}{\tau} & \frac{A_{\text{lat}}}{\tau} & 0 \\ 0 & \frac{B_{\text{lon}}}{\tau} & \frac{B_{\text{lat}}}{\tau} & 0 \end{bmatrix} \begin{bmatrix} \delta_{\text{thr}} \\ \delta_{\text{lon}} \\ \delta_{\text{lat}} \\ \delta_{\text{dir}} \end{bmatrix} \tag{3}$$

III. Results

A. Model Structure Determination

Two data sets, roughly 5 min in length, were furnished for this identification work. These flight tests are a subset of those used by Conroy et al. [12] and consist of excitation during hovering flight. One data set was used for model structure determination and parameter estimation, and the other data set was used to test the predictive capabilities of the identified models. The state-space model structure

Table 1 Measurement specifications

Measurement	Symbol	Source	Resolution	Variance	Unit
Time	t	FCS	25.600×10^{-6}	——	s
Control input	$\delta_{\text{thr}}, \delta_{\text{lon}}, \delta_{\text{lat}}, \delta_{\text{dir}}$	FCS	1.5000×10^{-3}	0.2426×10^{-3}	norm
Position	x, y, z	VPS	8.9072×10^{-6}	0.6128×10^{-3}	m
Orientation	ϕ, θ, ψ	VPS	——	7.8000×10^{-3}	rad
Translational velocity	u, v, w	VPS	——	0.2510×10^{-3}	m/s
Rotational velocity	p, q, r	VPS	——	1.2000×10^{-3}	rad/s
Rotor speed	Ω	VPS	——	0.2143×10^{-0}	rad/s

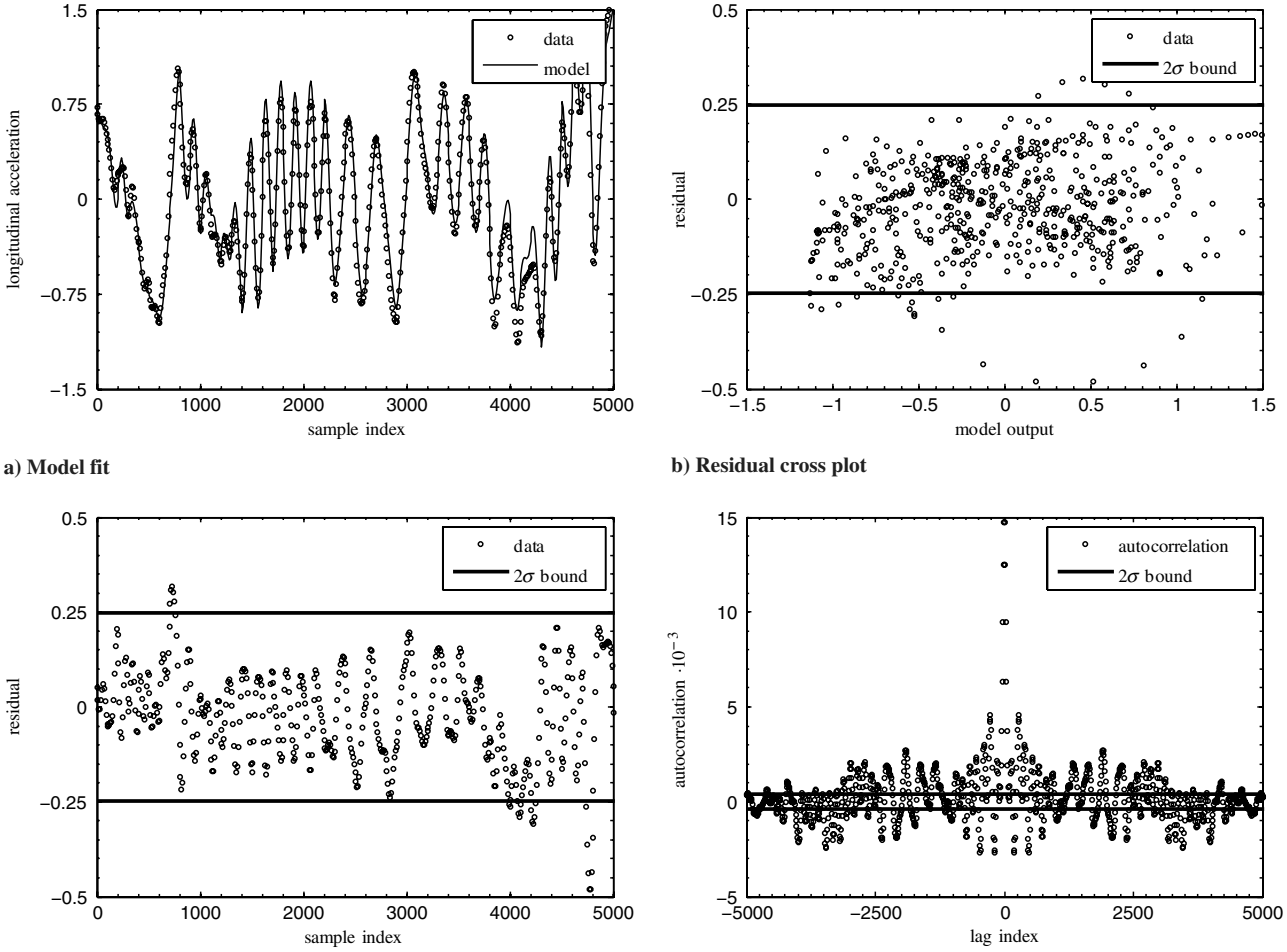

Fig. 4 Modeling results for the longitudinal velocity dynamics using the equation-error method in the time domain.

was postulated to describe the hover dynamics. The dynamics for the roll and pitch angles are analytical linearizations of the rotational kinematics about the trimmed hover condition. The dynamics for the roll and pitch rates are simplified from the hybrid model first proposed by Tischler and Cauffman [4] and later reduced as first-order tip path plane equations by Mettler [2]. The hybrid model has been used extensively in the literature and captures rotor dynamics and rotor/fuselage interactions using the states a and b, which represent the longitudinal and lateral flapping angles of the lumped rotor and stabilizer system. Stability derivatives M_a and L_b quantify

Table 2 Parameter estimates and color-corrected standard errors

Parameter $\boldsymbol{\theta}$	Time EE $\hat{\boldsymbol{\theta}} \pm s(\hat{\boldsymbol{\theta}})$	Frequency EE $\hat{\boldsymbol{\theta}} \pm s(\hat{\boldsymbol{\theta}})$	Time OE $\hat{\boldsymbol{\theta}} \pm s(\hat{\boldsymbol{\theta}})$	Frequency OE $\hat{\boldsymbol{\theta}} \pm s(\hat{\boldsymbol{\theta}})$
X_u	-0.2416 ± 0.0271	-0.2464 ± 0.0273	-0.4779 ± 0.0553	-0.2332 ± 0.0129
Y_v	-0.2801 ± 0.0915	-0.4296 ± 0.0582	-1.7289 ± 0.4903	-0.9635 ± 0.0691
Z_w	-0.4370 ± 0.1096	-0.4942 ± 0.0857	-2.0121 ± 0.4138	-1.1345 ± 0.0863
Z_Ω	-0.1161 ± 0.0077	-0.1488 ± 0.0075	-0.1358 ± 0.0209	-0.1627 ± 0.0074
L_v	——	——	-5.4637 ± 0.0209	-9.9087 ± 1.5383
L_b	——	——	$+1251.0 \pm 251.61$	$+925.16 \pm 189.15$
M_u	——	——	$+5.8088 \pm 0.3620$	$+5.4415 \pm 0.4073$
M_a	——	——	$+314.78 \pm 3.0747$	$+320.99 \pm 4.9541$
N_r	-3.2627 ± 0.2939	-4.8464 ± 0.3582	-13.483 ± 0.7080	-13.741 ± 0.9495
N_{thr}	-47.892 ± 5.7494	-56.213 ± 7.5060	-73.022 ± 9.5526	-83.585 ± 10.648
N_{dir}	-57.297 ± 3.4442	-74.746 ± 4.0758	-126.23 ± 4.2117	-142.63 ± 8.8034
T_Ω	-1.5656 ± 0.1302	-1.7016 ± 0.1290	-2.9477 ± 0.1672	-2.6525 ± 0.0872
T_{thr}	$+599.40 \pm 28.606$	$+704.91 \pm 25.620$	$+742.12 \pm 22.032$	$+760.21 \pm 18.972$
τ	——	——	$+0.1490 \pm 0.0035$	$+0.1399 \pm 0.0055$
A_b	——	——	-5.0356 ± 1.1274	-1.2211 ± 0.2997
A_{lon}	——	——	-0.1601 ± 0.0030	-0.1605 ± 0.0049
A_{lat}	——	——	-0.0625 ± 0.0024	-0.0618 ± 0.0039
B_a	——	——	$+1.1404 \pm 0.0630$	$+0.9913 \pm 0.0813$
B_{lon}	——	——	$+0.0962 \pm 0.0048$	$+0.1046 \pm 0.0078$
B_{lat}	——	——	-0.1507 ± 0.0061	-0.1304 ± 0.0098

the rotor torques on the fuselage, M_u and L_v represent speed derivatives, A_b and B_a capture cross-axis interactions in the rotor dynamics, τ is the rotor time constant, and A_{lon}, A_{lat}, B_{lon}, and B_{lat} are the gains from the pilot inputs to the flapping dynamics.

The structure of the remaining dynamic equations was determined using stepwise regression, a process where candidate regressors are swapped in and out of the model based in part on a variety of statistical metrics. For this process, the entire first data set was used and the regressor matrix consisted of the available measurements. Analysis was performed with the equation-error method in the frequency domain for computational efficiency and was also verified in the time domain for consistency. Frequency transforms were performed using a high-accuracy chirp-z transform [17] to obtain Fourier coefficients spaced at 0.005 Hz increments between 0.10 Hz and 3.00 Hz. The chosen spectral grid was finer than conventional rules of thumb [14], but resulted in better model fits. The acceleration due to gravity was modeled as a constant and its value was fixed. The terms X_u, Y_v, Z_w, and N_r are on-axis stability derivatives which represent, in part, the aerodynamic damping. The stability derivatives Z_Ω and T_Ω represent the effects of rotor speed perturbations to the vertical force on the fuselage and rotational torque on the main rotor. Control derivatives T_{thr}, N_{dir}, and N_{thr} are included to capture the throttle input effect on the rotor speed, the directional input effect on the yaw rate, and the mixing of the throttle setting to the yaw rate. The stability derivatives X_a, Y_b, and Y_{dir} are often used to model the longitudinal and lateral forces generated by the rotor and the side force from the tail rotor, but did not make a significant improvement to the model fit. Stability derivatives Z_r, N_v, N_w, and N_Ω contributed to the model accuracy but were discarded because parameter estimates were not consistent between the time and frequency domains and had large error bounds, due in part to collinearity in the data. The stability derivative T_r also increased the model accuracy, but was discarded because it coupled the eigenvectors in a nonintuitive manner. The only difference between the model in Eq. (3) and that used by Conroy et al. [12] is the N_{thr} term.

The residuals were also analyzed to evaluate the postulated model structure. Representative results are shown in Fig. 4 for the dynamics of the longitudinal velocity using the equation-error method in the time domain. For clarity, data points are decimated from 350 to 35 Hz. Figure 4a shows good agreement between the measured and predicted longitudinal accelerations. Model residuals are illustrated in Fig. 4c, which shows 2σ bounds around the unmodeled content at about 25% of the amplitudes experienced in the maneuver. The cross plot shown in Fig. 4b graphs the model outputs against the model residuals and indicates neither unmodeled nonlinearities nor nonstationary variances in the residuals. Figure 4d shows the autocorrelation of the residuals, which resembles white noise in that there is a strong peak at the zero lag index, but the remaining deterministic content outside of two standard deviations colors the residuals and requires additional corrections for the estimation of parameter error bounds [18].

B. Parameter Estimation

Estimates of the model parameters were found using the same data set used for model structure determination. The estimation methods minimize the cost functions

$$J(\boldsymbol{\theta}) = \frac{1}{2}\sum_{i=1}^{N_p} \boldsymbol{\nu}(i)^T \hat{\mathbf{R}}^{-1} \boldsymbol{\nu}(i) \tag{4}$$

$$J(\boldsymbol{\theta}) = \frac{1}{2}\sum_{i=1}^{m} \tilde{\boldsymbol{\nu}}(i)^\dagger \mathbf{S}^{-1} \tilde{\boldsymbol{\nu}}(i) \tag{5}$$

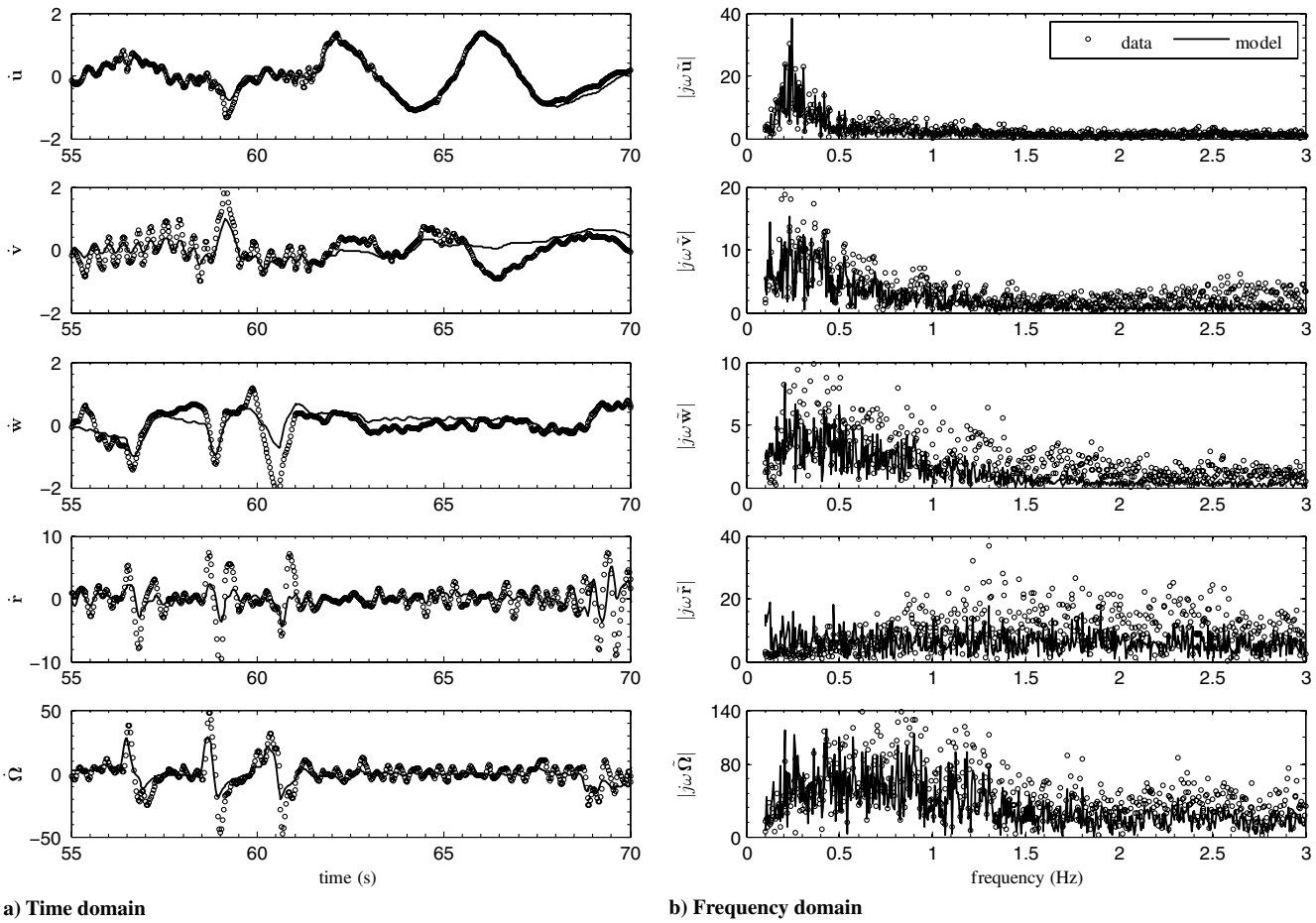

a) Time domain **b) Frequency domain**

Fig. 5 Measured and predicted state derivatives using the equation-error method.

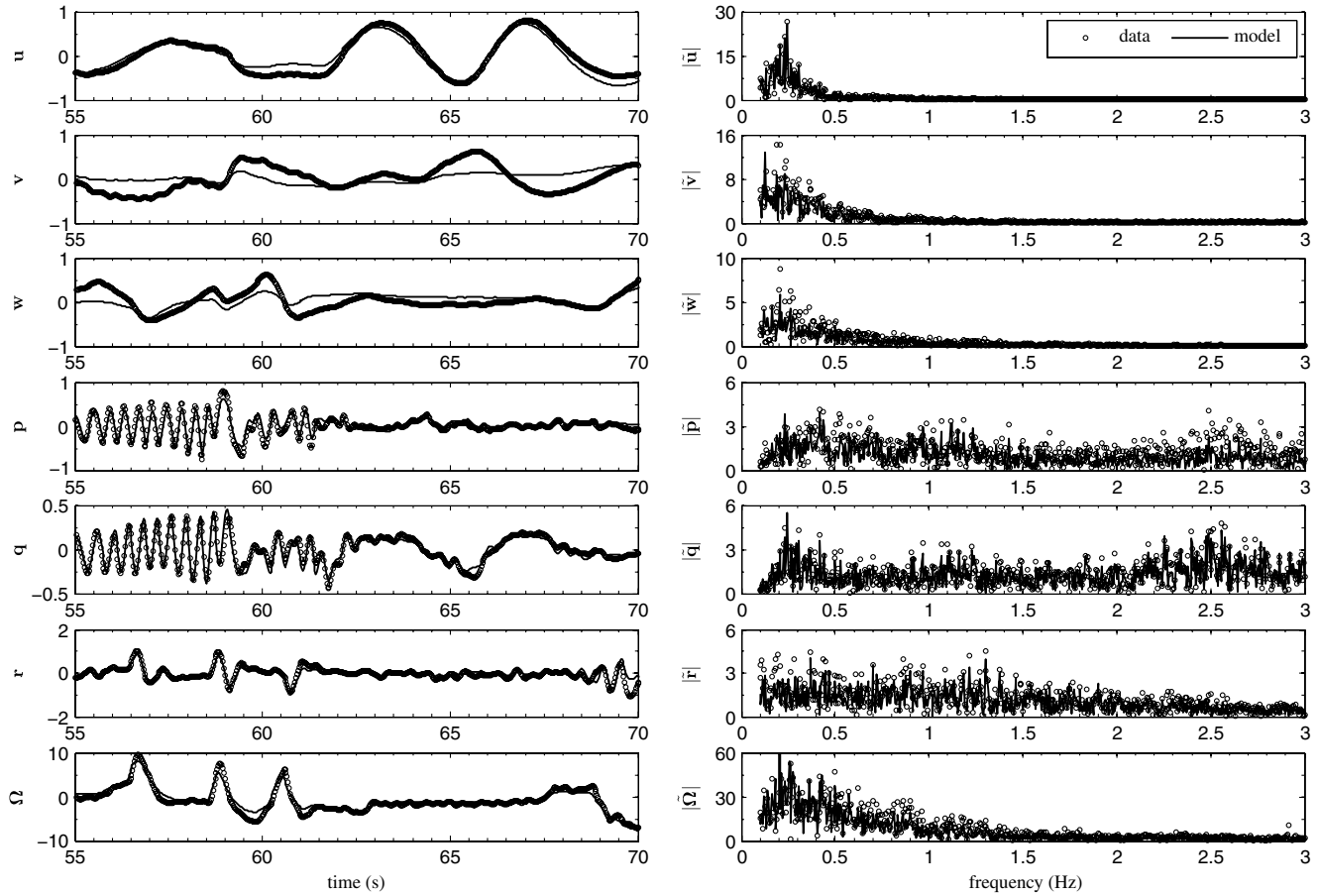

a) Times domain **b) Frequency domain**

Fig. 6 Measured and predicted outputs using the output-error method.

in the time and frequency domains, where N_p is the number of data points, m is the number of frequencies, $\boldsymbol{\nu}$ are the residuals, $\mathbf{R}$ is the residual covariance matrix, and $\mathbf{S}$ is the residual spectral density matrix. Equation-error residuals are the differences between the measured state derivatives and the model output for those state derivatives, whereas output-error residuals are the differences between the measured outputs and the predicted outputs. The equation-error method is a linear estimation problem with a deterministic solution, whereas the output-error method is a nonlinear estimation problem which requires an iterative solver. The identified parameter estimates with color-corrected standard errors are given in Table 2.

The equation-error method results are shown in Fig. 5 and are the first two data columns in Table 2. The equation-error method requires measurements of all the regressors and, because the flapping angles were not measured, the model parameters associated with the rotor dynamics could not be estimated. The parameters which could be estimated with equation-error were, for the most part, consistent between the time and frequency domains and were within two standard deviations of each other. A representative time domain fit is shown in Fig. 5a, in which the flight data has been decimated to 35 Hz for clarity, and the entire frequency domain fit is shown in Fig. 5b. The longitudinal velocity dynamics matched well, whereas the lateral and heave velocities did not capture the frequency content around 0.5 Hz, and the yaw rate and rotor speed dynamics did not capture the frequency content around 1.5 Hz.

The equation-error estimates were used as initial guesses for the parameters in the output-error method, except for the terms associated with the rotor dynamics, which were initiated according to Conroy et al. [12]. Results in both the time and frequency domain analyses achieved convergence within 25 iterations, although each iteration in the frequency domain analysis required far less time due to the number of data points used. The parameter estimates are the last two data columns of Table 2, which were generally consistent and fell within two standard deviations of each other. Model fits are shown in Fig. 6, in which a representative portion of the time domain results are shown, and which have been decimated to 35 Hz for clarity. Results show that the low-frequency dynamics of the lateral and heave velocity were not fully captured but, otherwise, the outputs matched well.

Table 3 Eigenvalues and modal characteristics.

	Time OE			Frequency OE		
Mode	Eigenvalue	ζ	ω, rad/s	Eigenvalue	ζ	ω, rad/s
Lateral flapping	$-4.00 \pm 39.5j$	0.10	39.7	$-3.84 \pm 31.6j$	0.12	31.9
Longitudinal flapping	$-2.57 \pm 15.5j$	0.16	15.7	$-3.17 \pm 16.7j$	0.19	17.0
Stable phugoid	$-1.35 \pm 0.67j$	0.90	1.51	$-0.88 \pm 0.98j$	0.67	1.32
Unstable phugoid	$+0.11 \pm 1.01j$	——	1.02	$+0.15 \pm 1.06j$	——	1.07
Heave subsidence	-2.01	1.00	2.01	-1.13	1.00	1.13
Yaw subsidence	-13.5	1.00	13.5	-13.7	1.00	13.7
Rotor speed subsidence	-2.95	1.00	2.95	-2.65	1.00	2.65

Generally, the results were consistent with each other and the parameter estimates were reasonable. From the standard errors given in Table 2, there was no clear distinction as to whether the time domain or frequency domain analysis produced more accurate estimates. The output-error results, however, generally had equal or larger error bounds than the equation-error results. The estimates of parameters Y_v, L_b, and L_v exhibited some scatter between the methods, which appeared to be due to a lack of excitation of the lateral velocity and the roll rate because the analogous longitudinal parameters X_u, M_a, and M_u were, for the most part, estimated consistently by the methods. Similarly, the scatter in the estimates of Z_w, T_Ω, and T_{thr} was attributed to small amounts of throttle and heave velocity excitation due to indoor space constraints. The scatter in the yaw rate parameters N_r, N_{thr}, and N_{dir} was attributed to the collinearity introduced by mixing the directional input with the throttle input and the yaw rate.

C. Modal Characterization

The modes of the aircraft are described by the eigenstructure of the system. Eigenvalues for the two models identified using output-error are given in Table 3 and are plotted along with those identified using the frequency-response method in Fig. 7. Polar plots of the eigenvalues showing the normalized magnitude and relative phase of the dominate directions in the state space are illustrated in Fig. 8.

The output-error models resulted in an eigenstructure consistent with that found using frequency responses. The first two modes are the lateral and longitudinal flapping modes, which are characterized by relatively fast and lightly damped oscillations between the roll rate and pitch rate. The second two modes are the stable and unstable phugoid modes, which are slower oscillations involving the longitudinal and lateral rotational velocities, translational velocities, and orientation angles. The last three modes are the heave, yaw, and rotor speed subsidence modes, which are slower first-order modes. These modes are consistent with the expected modes for larger aircraft in hover [2].

D. Model Validation

Model validation was performed by exciting the models with the control input time histories in the second data set, which was not used in the modeling process, and comparing model outputs with the

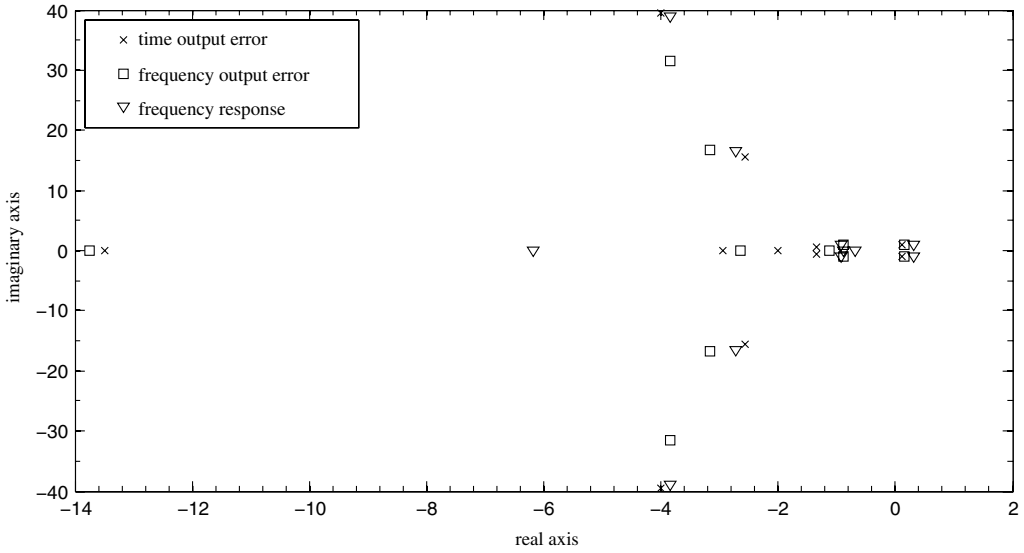

Fig. 7 Graphical representation of eigenvalues.

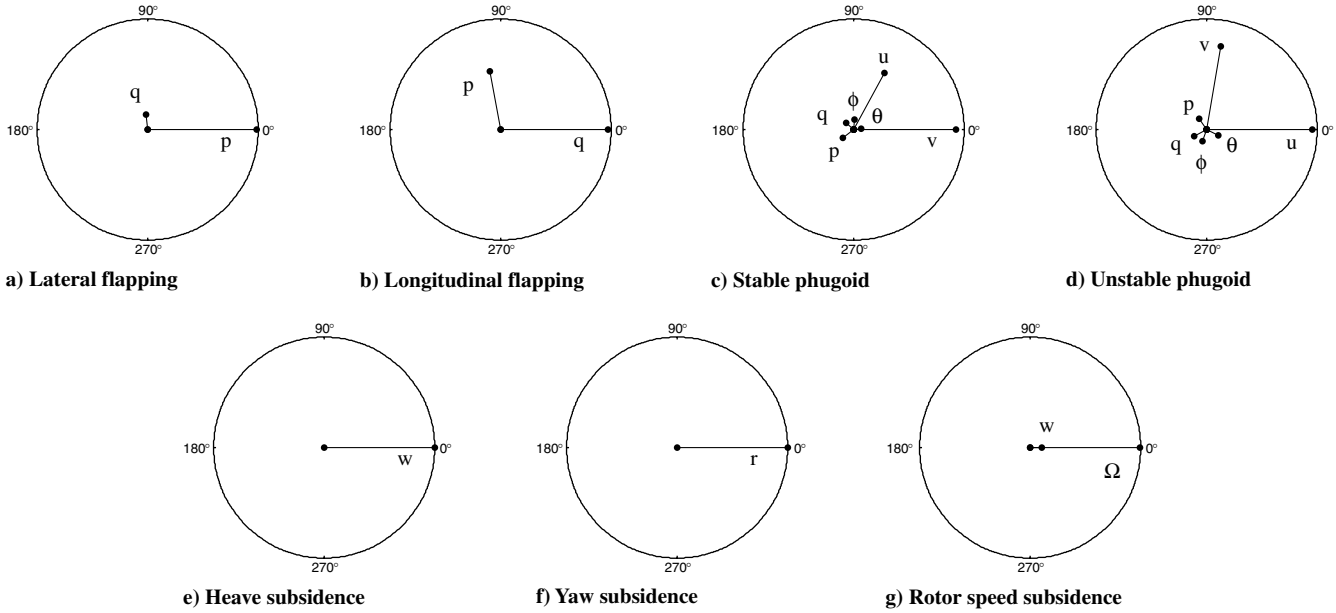

a) Lateral flapping **b) Longitudinal flapping** **c) Stable phugoid** **d) Unstable phugoid**

e) Heave subsidence **f) Yaw subsidence** **g) Rotor speed subsidence**

Fig. 8 Graphical representation of eigenvectors.

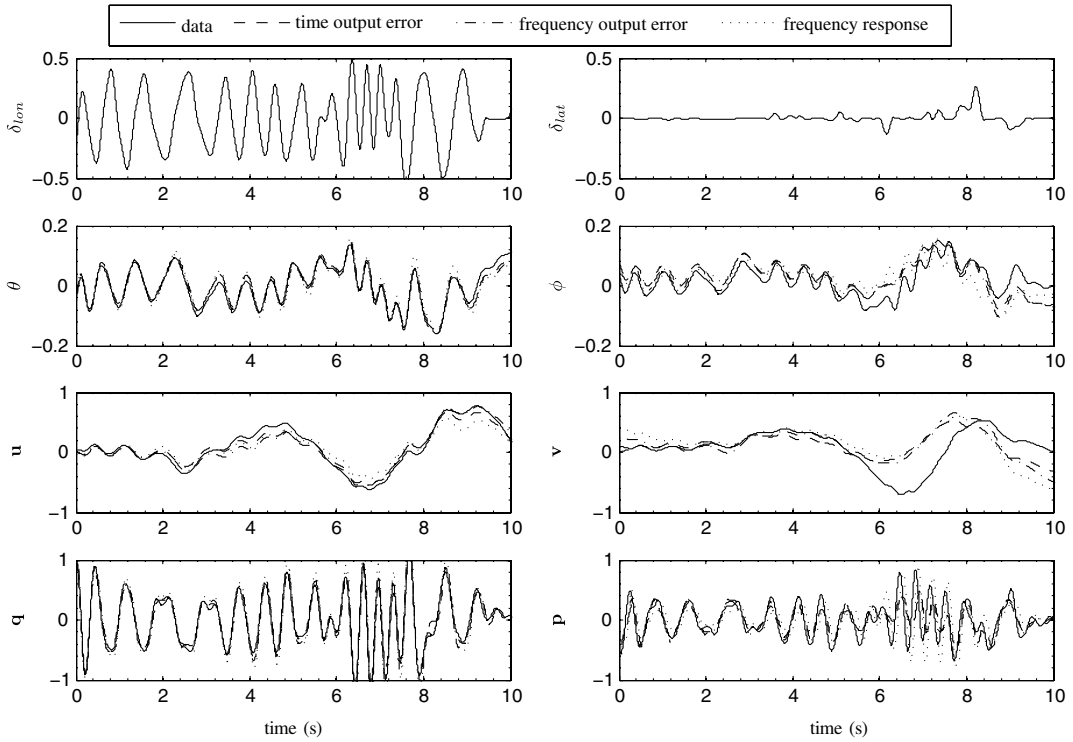

Fig. 9 Model prediction with longitudinal cyclic excitation.

measured outputs. Three segments of data were chosen for validation, which primarily excite the longitudinal, lateral, and heave/yaw/rotor dynamics, shown in Figures 9–11, respectively. Biases for the dynamic and output equations were estimated for the frequency domain output-error model and the frequency-response model using the output-error method [9].

Qualitatively, all three models predicted the measurements well, capturing the majority of the dynamics exhibited in the flight data and leaving only small differences between the models. Under longitudinal excitation, all three models predicted the longitudinal very well, but the output-error models underpredicted and the frequency-response model overpredicted the off-axis roll rate slightly, which led to drifts in the lateral velocity and roll angle. Under lateral excitation, the output-error models underpredicted and the frequency-response model overpredicted the roll rate and pitch rate amplitudes slightly, which led to slow drifts in velocities and orientation angles. Under throttle and directional excitation, measurements were predicted equally well by the three models, with the exception of the yaw rate by the frequency-response model, where errors due to not including the N_{thr} term were visible.

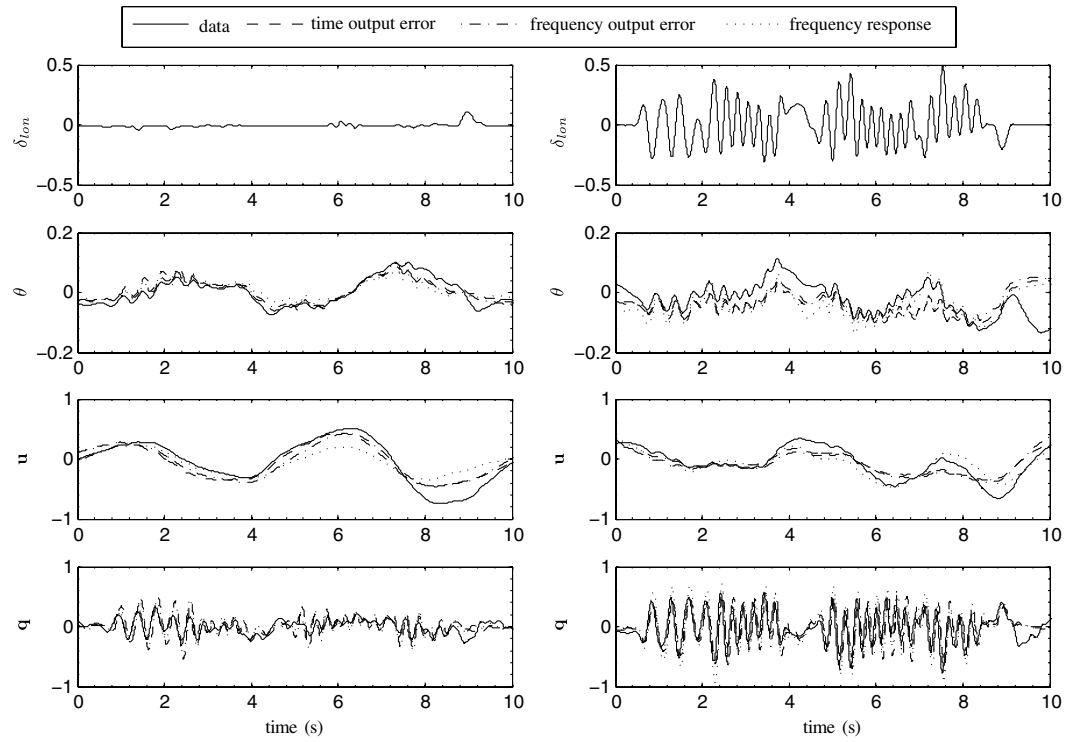

Fig. 10 Model prediction with lateral cyclic excitation.

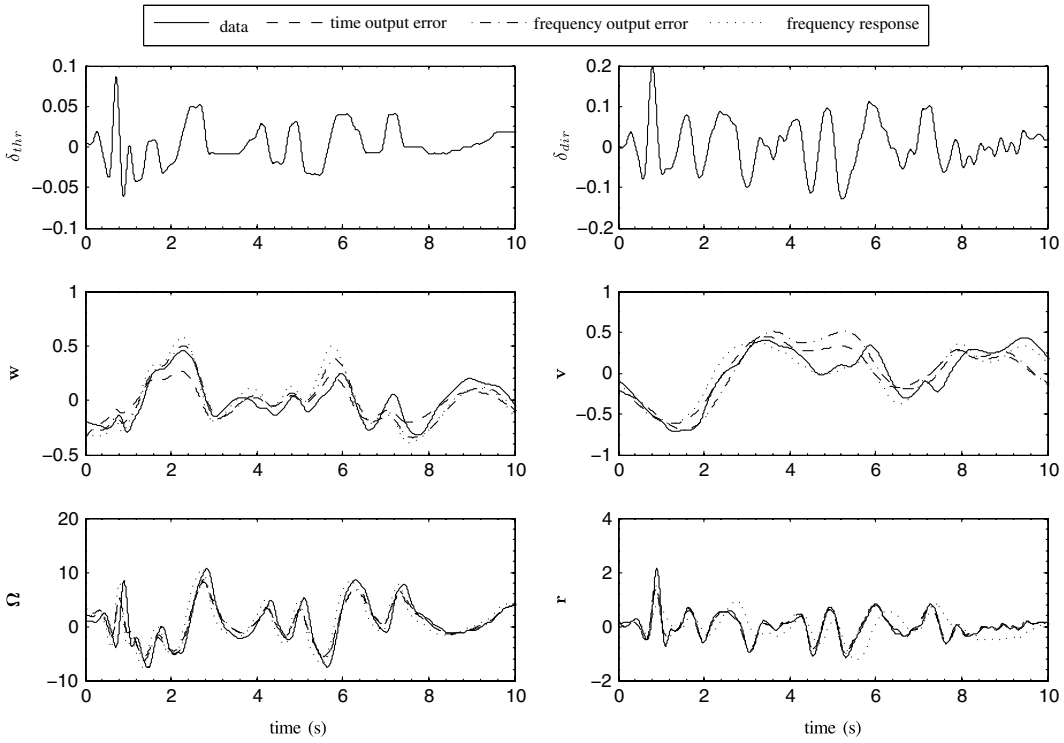

Fig. 11 Model prediction with throttle and directional excitation.

The model predictive capability can be quantified by metrics such as the Theil inequality coefficient (TIC) [9]

$$\text{TIC} = \frac{\sqrt{(1/N_p \cdot N_o)(\mathbf{z}-\mathbf{y})^T\mathbf{W}(\mathbf{z}-\mathbf{y})}}{\sqrt{(1/N_p \cdot N_o)\mathbf{y}^T\mathbf{W}\mathbf{y}} + \sqrt{(1/N_p \cdot N_o)\mathbf{z}^T\mathbf{W}\mathbf{z}}} \tag{6}$$

where N_o is the number of outputs and $\mathbf{W}$ is a weighting matrix, which was chosen as the inverse of the estimated residual covariance matrix. Guidelines for the TIC suggest that values less than 0.3 indicate a good predictive capability. The time output-error, frequency output-error, and frequency-response models had the following TIC values: 0.18, 0.16, and 0.26 for the longitudinal excitation, 0.36, 0.34, and 0.41 for the lateral excitation, and 0.29, 0.25, and 0.33 for the heave/yaw/rotor excitation, indicating that the frequency output-error model predicted the best, followed in small margins by the time output-error model and frequency-response model.

IV. Conclusions

This work presented the identification of a linear model describing the hover dynamics of a miniature electric helicopter for use in the design of control and state estimation algorithms. Flight data were collected in an indoor laboratory using an onboard flight control system and a visual positioning system. A model structure was postulated and model parameters were estimated in a two-step equation-error/output-error process. The eigenstructure and predictive capabilities of the identified models were compared with a frequency-response model.

With the exception of the control inputs, flight data used in the modeling process were derived from measurements obtained from the visual positioning system. These measurements had a significant effect on the modeling process. Derived measurements were cleaner than those obtained with MEMS avionics and did not require any corrections for kinematic consistency, calibration, or alignment, and ultimately resulted in better models. The visual positioning system is reliable and procedural to operate, whereas designing, building, and debugging custom hardware is often a long and tedious process.

The equation-error/output-error method was performed in both the time and frequency domains. The time domain analysis was significantly more time consuming than the frequency domain analysis because the flight data required filtering, low excitation levels needed large amounts of data, and colored residuals necessitated error-bound corrections. Frequency domain analysis, on the other hand, resulted in fast computation times of solutions that had slightly better predictive capabilities.

Two models were identified using a two-step equation-error/output-error method, and were found to have a similar model structure, parameter estimates, eigenstructure, and predictive capability as a model previously identified using the frequency-response method implemented with CIFER®. The overall consistency of these models provides good evidence that the identified models are accurate and that the methods used are appropriate for identifying miniature helicopters. The frequency domain output-error model was found to have slightly better prediction capability, as measured by the Theil inequality coefficient. All three models provide models accurate enough for controller and observer design.

Acknowledgments

The authors would like to thank the University of Maryland, the National Institute of Aerospace, and NASA Langley Research Center for their support in this research. Flight tests were conducted at the University of Maryland in the Autonomous Vehicle Laboratory. Many conversations with Eugene Morelli at the NASA Langley Research Center are acknowledged and greatly appreciated. Additionally, the authors would like to thank the members of the Morpheus Laboratory and Autonomous Vehicle Laboratory for their continued support and guidance.

References

[1] Theodore, C., Tischler, M., and Colbourne, J., "Rapid Frequency-Domain Modeling Methods for Unmanned Aerial Vehicle Flight Control Applications," *Journal of Aircraft*, Vol. 41, No. 4, July–Aug. 2004, pp. 735–743. doi:10.2514/1.4671

[2] Mettler, B., *Identification Modeling and Characteristics of Miniature*

Rotorcraft, Kluwer Academic, Norwell, MA, 2003.

[3] Leishman, J. G., *Principles of Helicopter Aerodynamics*, 2nd ed., Cambridge Aerospace Series, Cambridge Univ. Press, Cambridge, England, U.K., 2006.

[4] Tischler, M., and Cauffman, M., "Frequency-Response Method for Rotorcraft System Identification: Flight Applications to BO-105 Coupled Rotor/Fuselage Dynamics," *Journal of the American Helicopter Society*, Vol. 37, No. 3, 1992, pp. 3–17.

[5] Tischler, M., Leung, J., and Dugan, D., "Frequency-Domain Identification of XV-15 Tilt-Rotor Aircraft Dynamics in Hovering Flight," AIAA Paper 83-2695, 1983.

[6] Mettler, B., Tischler, M., and Kanade, T., "System Identification Modeling of a Small-Scale Unmanned Rotorcraft for Control Design," *Journal of the American Helicopter Society*, Vol. 47, No. 1, Jan. 2002, pp. 50–63.
doi:10.4050/JAHS.47.50

[7] Tischler, M., and Cauffman, M., "Comprehensive Identification from Frequency Responses, Vol. 1: Class Notes," NASA CP 10149, 1994.

[8] Tischler, M., and Cauffman, M., "Comprehensive Identification from Frequency Responses, Vol. 2: User's Manual," NASA CP 10150, 1994.

[9] Tischler, M., and Remple, R., *Aircraft and Rotorcraft System Identification: Engineering Methods with Flight Test Examples*, AIAA Education Series, AIAA, Reston, VA, 2006.

[10] Morelli, E., "Low-Order Equivalent System Identification for the Tu-144LL Supersonic Transport Aircraft," *Journal of Guidance, Control, and Dynamics*, Vol. 26, No. 2, March–April 2003, pp. 354–362.
doi:10.2514/2.5053

[11] Maine, R., and Illif, K., "Application of Parameter Estimation to Aircraft Stability and Control: The Output-Error Approach," NASA TR RP 1168, 1986.

[12] Conroy, J., Humbert, S., and Pines, D., "System Identification of a Rotary Wing Micro Air Vehicle," *Journal of the American Helicopter Society*, 2009 (to be published).

[13] Morelli, E., "System Identification Programs for Aircraft (SIDPAC)," AIAA Paper 2002-4704, 2002.

[14] Klein, V., and Morelli, E., *Aircraft System Identification: Theory and Practice*, AIAA Education Series, AIAA, Reston, VA, 2006.

[15] Graham, R., "Determination and Analysis of Numerical Smoothing Weights," NASA TR R-179, 1963.

[16] Morelli, E., "Practical Aspects of the Equation-Error Method for Aircraft Parameter Estimation," AIAA Paper 2006-6144, 2006.

[17] Morelli, E., "High Accuracy Evaluation of the Finite Fourier Transform Using Sampled Data," NASA Tech. Rept. TM 110340, 1997.

[18] Morelli, E., and Klein, V., "Accuracy of Aerodynamic Model Parameters Estimated from Flight Test Data," *Journal of Guidance, Control, and Dynamics*, Vol. 20, No. 1, 1997, pp. 74–80.
doi:10.2514/2.3997